Enhanced Osteogenic Efficacy of Phellodendron Amurense-Loaded Nanocomposite Scaffolds for Regeneration of Large-Scale Bone Defects

YUAN Xiuchen
Xuzhou Renci Hospital
Yao Fengpin
Xuzhou Renci Hospital
Li Dongfeng
Xuzhou Renci Hospital
Li Cunxiao
Xuzhou Renci Hospital
Meng Lei
Xuzhou Renci Hospital
Zhang Ye
Xuzhou Renci Hospital
Hao Wang
Xuzhou Renci Hospital
Yan Dong
Xuzhou Renci Hospital
Jun Shang
drshjun@163.com

Xuzhou Renci Hospital

Article

Keywords: Drug delivery, Composite scaffold, Polycaprolactone microspheres, Bone repair material

Posted Date: June 27th, 2025

DOI: https://doi.org/10.21203/rs.3.rs-6803190/v1

Additional Declarations: No competing interests reported.

Abstract

In this study, we report the design and fabrication of a novel biomimetic composite scaffold (PSGO) and systematically assess its potential for bone tissue engineering. The PSGO scaffold was fabricated using three-dimensional (3D) printing technology with a base matrix composed of polyethylene glycol (PEG), sodium alginate (SA), and gelatin (GEL). Obacunone-loaded polycaprolactone (OA@PM) microspheres were embedded within the scaffold to enable sustained drug release, thereby creating a structure with precise architecture and functional gradients. Comprehensive characterization of the scaffold's surface morphology, rheological properties, and drug release behavior was performed. In vitro experiments demonstrated that the PSGO scaffold significantly promoted the proliferation and differentiation of bone marrow mesenchymal stem cells (BMSCs), enhanced the expression of key osteogenic markers (RUNX-2 and OCN), and facilitated mineralized matrix formation. Furthermore, in vivo evaluation using a rat calvarial critical-size defect model—assessed via micro-computed tomography and histological analysis—confirmed its excellent osteogenic performance, with substantial new bone formation observed at both the defect margins and center. With its outstanding biocompatibility, osteoinductive capabilities, and controlled drug release properties, the PSGO scaffold offers a promising new approach for the clinical repair of large-scale bone defects.

1. Introduction

Bone defects resulting from traumatic accidents, bone tumor resections, and pathological fractures are significant clinical challenges that have long plagued orthopedic surgeons and materials researchers[1]. Autologous bone grafting, due to its superior biocompatibility and osteogenic properties, has long been regarded as the "gold standard" for bone defect repair. However, the application of autografts is limited by the scarcity of donor tissue and complications associated with the donor site, such as infection and chronic pain[2, 3]. Allogeneic bone partially alleviates the issue of autograft shortage but remains hindered by immune rejection and the potential risk of disease transmission, limiting its broader clinical application. Therefore, the development of novel biomaterials with excellent biological performance and osteogenic potential has become a key focus in the field of Bone Tissue Engineering (BTE).

With the rapid development of 3D printing technology, personalized and customized porous scaffolds have provided revolutionary solutions for the treatment of bone defects[3]. In recent years, the combination of hydrophilic scaffolds with drug-loaded microspheres has garnered significant attention. Hydrophilic scaffolds are known for their excellent biocompatibility and hydration properties, offering considerable advantages in promoting cell growth, enhancing cell adhesion, and accelerating tissue repair[4, 5]. Although significant progress has been made with bioactive substance-enhanced implants and gene engineering techniques to accelerate bone regeneration, challenges still persist in several areas, including controlled drug release, long-term stability, immune response, material compatibility, clinical application, and cost[6, 7]. As such, selecting appropriate bioactive materials for Bone Tissue Engineering (BTE) is critical for the successful integration and functionality of implants.

Polyethylene glycol (PEG), with its excellent hydrophilicity, biocompatibility, and low immunogenicity, has been widely used in drug delivery and tissue engineering, significantly prolonging the in vivo circulation time of drugs[8]. Sodium alginate (SA), as a natural polysaccharide, forms stable crosslinked networks but has limited efficacy due to the lack of cell adhesion sites[9]. When combined with PEG, it significantly improves its mechanical properties and degradation stability[10]. Gelatin (GEL), rich in RGD adhesion sequences, mimics the extracellular matrix and significantly enhances cell adhesion[11]. The synergistic interaction of PEG, SA, and GEL offers new possibilities for developing BTE scaffolds that combine superior bioactivity with functionality.

Obacunone (OA), a natural triterpenoid compound ($C_{26}H_{30}O_7$), has attracted considerable attention due to its osteogenic and anti-inflammatory properties. This compound, which has been validated through various studies in traditional Chinese medicine, has been shown through modern techniques to promote osteoblast proliferation, differentiation, and mineralization by activating signaling pathways such as BMP-2, β-catenin, and RUNX-2[12, 13]. However, the major challenge of OA is its poor solubility and low stability in vivo. To address this issue, we hypothesized that loading OA into polycaprolactone (PCL) microspheres (OA@PM) and combining it with scaffolds would provide a sustained-release drug delivery system, ensuring stable release of the drug and imparting biological functionality to the scaffold.

In this study, we propose a straightforward method to fabricate a composite hydrogel scaffold (PSGO) based on PEG/SA/GEL and loaded with OA@PM using 3D printing technology. This scaffold combines the excellent biocompatibility of PEG, the controllable crosslinked network of SA, the cell adhesion properties of GEL, and the sustained-release function of PCL microspheres, forming a functional bone tissue scaffold. First, we co-cultured the scaffold with osteoblasts to verify its non-toxicity and good biocompatibility. Moreover, in vitro experiments demonstrated that the scaffold promotes the expression of osteogenic genes, such as RUNX-2 and OCN, and exhibits good mineralization capacity. Further animal studies in a rat calvarial defect model revealed that after 4 weeks of implantation, the PSGO scaffold significantly enhanced bone formation (Scheme 1). Overall, this study innovatively combines plant-derived bioactive compounds with modern bone tissue engineering techniques, offering new insights and possibilities for the clinical repair of large bone defects.Materials and Methods.

Scheme 1. Schematic Illustration of the Preparation of Composite Scaffolds Loaded with Obacunone and Their Application in Bone Regeneration

2. Materials and methods

2.1 Materials

Gelatin (GEL), sodium alginate (SA), and polyethylene glycol (PEG) used in this study were purchased from Sigma-Aldrich (St. Louis, MO, USA). Obacunone (OA) and polycaprolactone (PCL) were obtained from Yuan Ye Biotechnology Co., Ltd. (Shanghai, China). Dichloromethane (DCM) and dimethyl sulfoxide (DMSO) were supplied by Alfa Aesar (Haverhill, MA, USA). Phosphate-buffered saline (PBS) was sourced

from Gibco (Grand Island, NY, USA). Dulbecco's Modified Eagle's Medium (DMEM), fetal bovine serum (FBS, 5% v/v), and penicillin-streptomycin solution (P/S, 1% v/v) were provided by Invitrogen (Carlsbad, CA, USA).

2.2 Methods

2.2.1. OA@PM Microsphere Preparation

The preparation of OA@PM microspheres was based on the previously reported method by our team, with appropriate optimizations[14]. The microspheres loaded with Obacunone (OA) were fabricated using an oil-in-water (O/W) emulsion-solvent evaporation technique. Briefly, 110 mg of Polycaprolactone (PCL) was dissolved in 5 mL of dichloromethane, and the solution was sonicated for 1.5 hours at 130 W and 35 Hz in a water bath. Next, 22.73 mg of Obacunone was added to the solution and thoroughly mixed. The resulting solution was then dropwise added to a 3.0% (w/v) Polyvinyl alcohol (PVA) solution to form an emulsion. The emulsion was centrifuged at 15,000 rpm for 45 minutes at room temperature. The final product was washed three times with distilled water, followed by lyophilization under low temperature to obtain the nanospheres, which were stored at 4°C for further use. For the preparation of PCL microspheres without OA, the same procedure was followed, with no further elaboration.

2.2.2. Scaffold Preparation

A suitable amount of PEG, SA, and GEL powders were weighed and added to a beaker containing distilled water. The mixture was stirred at 50°C using a magnetic stirrer until completely dissolved, resulting in solutions with concentrations of 3.5%, 5.5%, and 4.5%, respectively. The prepared solutions were then mixed in a 1:1:1 ratio and loaded with OA@PM. The mixture was stirred at 250 rpm for 3 hours to ensure uniform mixing, producing the bio-ink. The bio-ink was printed using a 3D printer (DD135-N nozzle) based on a pre-set CAD software program. The nozzle diameter was 0.33 mm, with a printing speed of 3.6 mm/s and pressure ranging from 0.35 to 0.45 MPa. The final composite scaffold had a size of 7.0 mm in diameter (⌀) and 2.16 mm in height (h). Parameters were adjusted based on the specific printing conditions for each batch. PSGO composite scaffolds containing OA@PM were prepared as the experimental group, while PSG scaffolds without OA@PM served as the control group. The printed scaffolds were then crosslinked overnight in a 2.5% anhydrous calcium chloride solution. After chemical crosslinking, the scaffolds were dried and sterilized with ethylene oxide before being stored for further use.

2.2.3. Characterization of Scaffold and OA@PM Microspheres

The microstructure of the scaffolds and OA@PM microspheres was evaluated using a scanning electron microscope (SEM, JSM-6360LA, Japan). Additionally, OA@PM (60 mg) was dispersed in 15 mL of distilled water using ultrasound treatment (360 W, 15 s). The particle size distribution of OA@PM was measured by dynamic light scattering (DLS).

2.2.4 Fourier Transform Infrared (FTIR) Analysis

To prepare the samples, PSG/PSGO scaffolds were ground into a fine powder and mixed with 250 mg of potassium bromide. The mixture was then compressed into pellets and scanned in the range of 400 ~ 4000 cm^{-1} with a resolution of 4 cm^{-1}.

2.2.6. Rheological Analysis of Hydrogel Ink

The rheological properties of the hydrogel ink were analyzed using a rheometer. Briefly, the hydrogel ink was spread onto the plate of the rheometer. Small amplitude oscillatory shear tests were performed at a strain amplitude of 5% within a shear rate range of 0 s^{-1} to 100 s^{-1} at room temperature. The storage modulus (G') and loss modulus (G") were recorded within the temperature range of 15°C to 45°C.

2.2.7. Water Contact Angle Measurement of Scaffolds

To measure the water contact angle of the scaffolds, the hydrogel scaffold was placed on a glass slide to form a flat surface. A 2 μL water droplet was dropped vertically onto the scaffold, and the contact angle was measured using a contact angle goniometer at the moment the droplet landed on the surface.

2.2.8. Water Absorption Rate of Materials

Three scaffolds from each group were randomly selected and immersed in PBS for 24 hours. After removing excess water with absorbent paper, the scaffolds were weighed. The water absorption rate was calculated using the following formula (n = 3):

$$Water\ absorption\ ratio\ (\%) = \frac{W_{wet} - W_{dry}}{W_{dry}} \times\ 100\ \%$$

Where W_{wet} is the weight of the scaffold after 24 hours of immersion, and W_{dry} is its initial dry weight.

2.2.9.Drug Release Rate

The OA@PM microspheres and PSGO scaffolds were separately placed in 35 mL centrifuge tubes containing PBS (pH = 7.4) and incubated at 37°C. At specified time intervals, 2 mL of supernatant was withdrawn and replaced with fresh PBS to maintain a constant volume of 35 m L. The drug release rate was determined using UV-Vis spectroscopy. The cumulative release percentage was calculated using the following formula (n = 3):

$$OA\ released = \left(\frac{measured\ OA\ released}{total\ OA\ amount}\right) \times\ 100\%$$

2.3.0. Cell Culture

Before the experiment, the composite scaffolds were sterilized using ethylene oxide gas. Mouse bone marrow mesenchymal stem cells (BMSCs) (ATCC; Chinese Academy of Sciences, Shanghai, China) were utilized for cell culture studies. The BMSCs were maintained in a humidified incubator at 37°C with 5% CO_2. Cells were cultured in Dulbecco's Modified Eagle Medium (DMEM) supplemented with 10% fetal

bovine serum (FBS) and 1% (v/v) penicillin-streptomycin (P/S). The culture medium was refreshed every 2–3 days. When cell confluence reached approximately 80%, the cells were passaged for subsequent experiments. In accordance with the guidelines of the International Organization for Standardization (ISO 10993-12), scaffold extracts were prepared. Briefly, sterile scaffolds were incubated in serum-free DMEM at a concentration of 0.1 g/mL for 48 hours at 37°C. After incubation, the supernatant was collected, filter-sterilized, and then supplemented with 10% FBS and 1% P/S. The resulting elution solution was stored at 4°C until further use.

2.3.1. Cell Biocompatibility Assessment

Cell viability was assessed using the CCK-8 assay to evaluate the effect of the hydrogel scaffolds on cell proliferation. BMSCs were seeded in a 96-well plate at a density of 4×10^3 cells/well and incubated with the scaffold eluates for 1, 3, and 5 days, as per the manufacturer's instructions. After incubation, absorbance at 450 nm was measured using a microplate reader. To further evaluate biocompatibility, Live/Dead staining was performed. BMSCs were seeded at 3×10^4 cells/well in a 24-well plate and allowed to adhere. After the medium was aspirated, different scaffold eluates were added to the cells. After 48 hours of incubation with the eluates, Live/Dead staining reagents were applied according to the manufacturer's instructions, and images were captured using an inverted fluorescence microscope.

2.3.2. Real-time Quantitative PCR (RT-qPCR)

After co-culturing the materials with BMSCs for 7 days, total RNA was extracted from the cells using TRIzol reagent (Invitrogen, USA) according to the manufacturer's instructions. cDNA was synthesized using a reverse transcription kit (Vazyme, China) as per the provided protocol. Real-time quantitative PCR was performed using SYBR Green PCR Master Mix (Vazyme, China) on a real-time PCR system. Table 1 lists the primers used for osteogenesis-related genes in the RT-qPCR assays.

Table 1
RT—qPCR primer sequences for osteogenesis-related genes

Gene	Forward	Reverse
GAPDH	5'-CACCACCAACTGCTTAGC-3'	5'- TCACCACCTTCTTGATGTC-3'
RUNX-2	5'-CTGCAAGCAGTATTTACAACAGAGG-3'	5'-GGCTCACGTCGCTCATCTT-3'
OCN	5'-GGC AGC CTC TGA TTG TGT CC-3'	5'-TAT ATC CAC TGC CTG AGC GG-3'

2.3.3. Alkaline Phosphatase and Alizarin Red Staining

The osteogenic induction medium consisted of basal medium, 100 nM dexamethasone, 10 mM β-glycerophosphate, and 50 μg/mL ascorbic acid. BMSCs (5×10^4 cells) were seeded in 6-well plates, and after cell attachment, the culture medium was replaced with the extract solution from different scaffolds. After 2 days of incubation with the extract solution, the medium was switched to osteogenic induction medium and cultured for 7 days. Alkaline phosphatase (ALP) staining was performed using an

ALP staining kit according to the manufacturer's instructions, with incubation for 6–7 hours. Similarly, BMSCs were cultured for 14 days and subjected to Alizarin Red S staining. Cell images were captured using an optical microscope for further analysis.

2.3.4. In Vivo Experiment

A rat calvarial defect model was established using 15 male SD rats (8 ~ 10 weeks old, 200 ~ 230 g). The rats were randomly assigned into three groups (n = 5): blank control, PSG, and PSGO. Anesthesia was induced using 3% pentobarbital (100 mg/kg). A circular calvarial defect (8 mm in diameter) was created using an electric drill, and the scaffolds were implanted into the defect site. After 4 weeks, all rats were euthanized for in vivo bone formation evaluation. The incision was then sutured. All animal procedures were conducted in accordance with the Institutional Animal Care and Use Committee (IACUC) guidelines and approved by Jiangsu Science Standard Medical Testing Co., Ltd. (IACUC23-0048).

2.3.5. Micro-CT Scanning and Histological Evaluation

The calvarial defect repair was evaluated using a SkyScan 1276 micro-CT scanner 4 weeks post-surgery (n = 3). The bone volume fraction (BV/TV) and trabecular number (Tb.N) were assessed. The calvarial bones were decalcified using 15% ethylenediaminetetraacetic acid (EDTA) for 30 days, with solution changes every 2 ~ 3 days. The samples were then dehydrated, embedded in paraffin, and sectioned to 5 μm thickness. Hematoxylin and eosin (H&E) staining and Masson's trichrome staining were performed following the manufacturer's instructions. Sections were examined under an optical microscope. For immunofluorescence staining, tissue sections were blocked with 5% BSA and 0.25% Tween 20 in PBS. Primary antibodies against osteopontin (OPN) (1:250, Abcam) and Alexa Fluor 488-labeled goat anti-rabbit secondary antibodies (1:500) were applied.

2.3.6. Data Analysis

All data are presented as the mean ± standard deviation (Mean ± SD). The significance between two groups was assessed using Student's t-test, while one-way analysis of variance (ANOVA) was used for comparisons among three or more groups. Statistical significance was defined as $P < 0.05$ (*) and $P < 0.01$ (**). Graphs were generated using GraphPad Prism 9.1 and Origin 8.0 (OriginLab) software.

3. Results

3.1. Scaffold and Microsphere Characterization

As shown in Fig. 1A, the scaffold exhibits a uniform pore size distribution. Scanning electron microscopy (SEM) images reveal a wrinkled surface on the scaffold, which enhances cell adhesion and proliferation. Particle size analysis of the microspheres indicated a distribution predominantly between 10 ~ 50 μm, with a relatively uniform size distribution.

3.2 FTIR Analysis

As shown in Fig. 2A, the FTIR spectra of scaffolds from all groups exhibit similar characteristic peaks. The broad absorption band around 3277 cm^{-1} corresponds to the O–H stretching vibration, indicating the presence of hydroxyl groups. The peak at 1600 cm^{-1} is attributed to the carboxylate (COO^-) groups in sodium alginate (SA) and the amide I band (C = O stretching) in gelatin, confirming the successful incorporation of both SA and GEL[15]. Notably, the distinct peak at 983 cm^{-1} is associated with Obacunone, suggesting its successful encapsulation within the scaffold. These characteristic absorption bands collectively validate the composite composition and demonstrate the effective integration of Obacunone into the scaffold matrix.

3.3. Physicochemical Properties of the Scaffolds

The printability of the bio-ink was assessed through rheological analysis. As shown in Fig. 2B, the storage modulus (G') and loss modulus (G") of both scaffolds gradually decreased with increasing temperature, regardless of temperature changes. The trends of both groups were similar. The hydrophilicity and water absorption rates of the two scaffolds were comparable (Fig. 2C and D, $^*P < 0.05$). In the drug release rate test, on Day 1, the drug release rates of OA@PM and PSGO were 13.66 ± 1.60% and 4.38 ± 1.20%, respectively. By Day 6, the drug release rate of OA@PM reached 53.56 ± 5.61%, while PSGO showed a release rate of 30.23 ± 3.39%. Overall, PSGO exhibited a significantly slower drug release compared to OA@PM. On Day 12, the release rates of OA@PM and PSGO were 72.38 ± 3.22% and 53.70 ± 5.63%, respectively (Fig. 2E). These results suggest that the PSGO scaffold effectively delays drug release, exhibiting superior controlled-release performance.

3.4. Biocompatibility Assessment of the Scaffolds

Cell viability was evaluated using the CCK-8 assay to assess the impact of the scaffolds on cell activity. As shown in the figure, no significant differences ($^*P < 0.05$) were observed between the blank group, the control group (PSG), and the experimental group (PSGO) on Day 1, Day 3, and Day 5 of co-culturing with the scaffolds. After co-culturing the scaffolds with BMSCs for 48 hours, Live/Dead cell fluorescence staining revealed a large number of live cells emitting green fluorescence, with only a few dead cells emitting red fluorescence. These results indicate that both groups of hydrogel scaffold we constructed exhibit good biocompatibility with no apparent toxicity.

3.5. Effect of Scaffolds on Osteogenic Differentiation of BMSCs

After co-culturing the scaffolds with BMSCs for 3 and 7 days, the expression of osteogenic markers RUNX-2 and OCN was assessed using RT-qPCR. The results showed that the gene expression levels in the PSGO group were significantly higher than those in the PSG group.Alkaline phosphatase (ALP) staining was used to evaluate the osteogenic differentiation activity of the cells. The results indicated that the PSGO scaffold group, loaded with OA@PM, exhibited significantly higher ALP activity, with the stained regions displaying a more intense blue-violet color compared to the PSG and blank groups.

Alizarin Red S (ARS) staining was performed to assess mineralization levels. The results showed a significant deposition of calcium nodules in the PSGO scaffold group, with the stained areas appearing a darker red. In contrast, the staining in the other two groups was relatively lighter, indicating lower levels of mineralization. These results suggest that the OA@PM-loaded PSGO scaffold significantly promoted the late-stage mineralization capability of BMSCs.

3.6. Micro-CT and Histological Evaluation

Four weeks post-surgery, the calvarial defect repair in rats was evaluated using Micro-CT scanning. The results showed that the blank control group only formed a small amount of fibrous tissue at the defect site. Although the PSG group did not contain Obacunone, the scaffold material exhibited some promotive effects on bone-fiber generation. However, in both groups, new bone formation was primarily confined to the edges of the defect, with limited quantity and a relatively modest repair outcome. In contrast, the PSGO group demonstrated significant advantages in bone repair, especially in the central region of the defect, where a large amount of new trabecular bone was observed filling the defect area. Quantitative analysis revealed that the bone volume fraction and trabecular number in the PSGO group were significantly higher than those in the blank control and PSG groups, with statistically significant differences ($*P < 0.05$).

4. Discussion

In the field of tissue engineering, the controlled release of bioactive substances from materials is a critical factor in tissue repair and regeneration. Controlling drug release helps establish the appropriate local drug concentration[16]. Current studies have explored various strategies to enhance scaffold functionality, such as material combination, RNA loading, and drug grafting[6, 17, 18]. In previous studies, our team grafted Leonurus onto scaffolds via amide bonds for sustained drug release and combined Pioglitazone with PLGA microspheres for slow drug release[19, 20]. However, these methods face challenges such as unstable release of bioactive substances, degradation, and the local acidic environment caused by the carrier materials. Jung-Ju Huang and colleagues reported that the metabolites of PLGA scaffolds create an acidic environment locally, which inhibits cell viability and tissue regeneration, ultimately reducing osteogenic efficiency[1]. To address these issues, we introduced Polycaprolactone (PCL), which degrades slowly and generates 6-hydroxycaproic acid, a weak acid that does not significantly lower the local pH[21]. In our previous work, our research group successfully employed PCL as a carrier to load-Curculigoside, achieving sustained drug release that induces and promotes osteogenesis[14].

Obacunone (OA), a small molecule derived from the natural plant genus Phellodendron, has been proven to possess multiple biological activities, including anti-inflammatory, antioxidant, anti-osteoporotic, and osteogenic effects, particularly in bone tissue repair. For instance, Jianbo He et al. showed that OA can alleviate bone loss by inhibiting RANKL-induced osteoclast differentiation, demonstrating its anti-osteoporotic effects[12]. Moreover, Kyung-Ran Park et al. found that OA promotes the BMP signaling

pathway, increases the phosphorylation of Smad1/5/8, and upregulates RUNX2 expression, which are key steps in osteoblast differentiation and bone formation[13]. This multi-target osteogenic regulatory mechanism indicates that OA not only inhibits bone resorption but also promotes bone formation. Therefore, we hypothesized that combining OA with hydrogel scaffolds could significantly enhance the bone-inductive effects of the scaffold. Additionally, Jinhee Kim et al. pointed out that OA has antitumor activity, especially by inhibiting the p38 MAPK signaling pathway in breast cancer cells to exert anti-proliferative effects[22]. This suggests that OA also holds potential for application in bone tumors and related bone lesions.

In this study, we proposed a simple approach by combining PEG, SA, and GEL, and integrating OA with drug delivery technology. We used the emulsion-evaporation method to prepare OA@PM microspheres and successfully fabricated PSGO bio-ink. These improvements are consistent with Shijie Fan et al.'s findings in PLGA microsphere systems, confirming the universality of the emulsion-evaporation method for drug-loaded microspheres[20]. Similarly, other studies have used oil-in-water (O/W) emulsion solvent evaporation techniques to prepare PLGA microspheres loaded with Dexamethasone, which also exhibited good drug release profiles[23]. SEM analysis revealed that the scaffold surface is rough with uniform pores, which enhances cell nutrient exchange and drug release. The surface area, roughness, and pore structure of the scaffolds affect cell adhesion[24].

Through rheological and drug release experiments, we compared the performance of PSG and PSGO bio-inks. Rheological analysis revealed that the viscoelasticity of both materials decreased with increasing temperature, indicating that the scaffolds tend to soften under elevated temperatures and exhibit enhanced flowability. This phenomenon not only reflects the printability of the materials under different thermal conditions but also implies changes in structural stability. For 3D printing applications, appropriate thermoresponsive behavior facilitates bio-ink flow control and interlayer fusion during the printing process. However, it also highlights the need to ensure adequate mechanical stability of the scaffold at physiological temperatures, which will be evaluated in our future studies[25]. Additionally, the high water absorption and excellent drug loading and release properties of both scaffolds likely play a critical role in bone regeneration. Hydrophilic scaffolds not only help maintain a moist local environment, promoting cell migration and nutrient exchange, but also provide sustained support for growth factors or other bioactive substances during the repair process[26]. The hydrophilicity and water absorption rates of both scaffolds showed no significant differences, which can be attributed to the relatively small proportion of hydrophobic PCL in the overall formulation. Litong Wang's gene-activated matrix technology not only maintains a moist environment but also increases the local concentration of active factors, achieving in situ repair. This is similar to the ideal results we aim for in our research[27]. However, in terms of drug release, OA@PM microspheres exhibited rapid release within the first 24 hours (13.66 ± 1.60%), which is related to the dissociation of the drug adsorbed on the surface. In contrast, the PSGO scaffold significantly reduced the burst release rate due to the spatial confinement effect of the polymer matrix (4.38 ± 1.20%, $^{*}P < 0.01$). By Day 6, the cumulative release rate difference between the two groups increased to 23.33% (OA@PM: 53.56 ± 5.61% vs. PSGO: 30.23 ± 3.39%), and by Day 12, the release rates

of OA@PM and PSGO were 72.38 ± 3.22% and 53.70 ± 5.63%, respectively ($^{*}P < 0.05$). This sustained-release property is likely due to the dual barrier effect of the microspheres and matrix, which prolongs the diffusion path of the drug. Literature reports also support this[28].Live/Dead staining and CCK-8 assays confirmed that the composite scaffolds had no apparent toxicity and promoted cell growth and proliferation. ALP and ARS staining, which are widely used to assess early and late osteogenic capabilities in bone tissue engineering, showed that the PSGO scaffold significantly enhanced both early and late osteogenic differentiation[29]. RUNX-2 and OCN, key osteogenic markers at early and late stages of osteogenesis, were significantly upregulated in the PSGO group compared to the control group[30]. These results, consistent with ALP and ARS staining, further validate the osteoinductive properties of the PSGO scaffold.

We hypothesize that the scaffold's osteoinductive effect is enhanced due to the combination of OA@PM with the hydrogel matrix. The unique bioactivity of OA interacts with the extracellular matrix, enhancing cell adhesion, proliferation, and differentiation, thus providing a favorable microenvironment for BMSC osteogenic differentiation. Compared to the PSG scaffold, the PSGO scaffold exhibited a significant increase in bone volume fraction and trabecular number, which could be attributed to the multifaceted effects of the OA-loaded scaffold. Furthermore, Masson’s trichrome and H&E staining further confirmed that the PSGO scaffold exhibited superior osteogenic activity around the scaffold compared to the other two groups. These results are consistent with our gene expression, ALP, and ARS findings.

In conclusion, through adjusting the microenvironment and endowing scaffolds with powerful bioactivity, the osteoinductive and angiogenic effects of the scaffold were enhanced, improving its potential as a bone tissue regeneration material. This functionality makes PSGO scaffolds highly promising for future applications in bone tissue repair and regeneration.

5. Conclusion

In this study, we successfully developed a biomimetic PSGO composite scaffold with excellent physicochemical properties and osteoinductive potential. In vitro experiments demonstrated that the scaffold exhibited outstanding biocompatibility and biosafety, significantly upregulated the expression of osteogenesis-related genes, and promoted mineralized matrix formation by osteogenic cells. In vivo, the implantation of the PSGO scaffold into a rat calvarial critical-sized defect model for 4 weeks resulted in a substantial increase in new bone formation, as confirmed by micro-CT and histological analyses. The incorporation of obacunone (OA) further enhanced the scaffold’s osteogenic performance while maintaining favorable biocompatibility. These results suggest that the PSGO scaffold is a promising candidate for clinical applications in the repair of large bone defects.

Declarations

Ethical Statement

All experimental procedures involving animals were conducted in strict compliance with the ARRIVE guidelines 2.0 (Animal Research: Reporting of In Vivo Experiments). The study protocol was reviewed and approved by the Institutional Animal Care and Use Committee (IACUC) of Jiangsu Science Standard Medical Testing Co., Ltd. (Approval No. IACUC23-0048).

Conflict of interest

The authors have no conflict of interest.

Funding

This work was supported by the Xuzhou Municipal Science and Technology Program (Grant No. XWKYHT20240020).

Author Contribution

X.Y. drafted the original manuscript. F.Y. contributed to the conceptual framework, supervised the project, and assisted with manuscript review and editing. D.L. provided essential resources. C.L. offered additional conceptual insights and resource support. L.M. and Y.Z. also contributed important resources. J.S., Y.D., and H.W., as corresponding authors, provided critical supervision and further conceptual guidance. All authors reviewed and approved the final manuscript.

Acknowledgements

This study was supported by the Xuzhou Science and Technology Program (XWKYHT20240020).

Data Availability

The datasets used and/or analyses during the current study available from the corresponding author on reason-able request.

References

1. Kim, D. S. et al. Advanced PLGA hybrid scaffold with a bioactive PDRN/BMP2 nanocomplex for angiogenesis and bone regeneration using human fetal MSCs. *Sci. Adv.* **7** (50), eabj1083. 10.1126/sciadv.abj1083 (2021). From NLM PubMed-not-MEDLINE.
2. Guo, K. et al. Polypeptide Promotes Osteogenesis in Jaw Bone Defect Repair by Inhibiting Inflammatory Reactions. *Front. Bioeng. Biotechnol.* **10**, 916330. 10.3389/fbioe.2022.916330 (2022).

From NLM PubMed-not-MEDLINE.

3. Dahabreh, Z. et al. Ability of bone graft substitutes to support the osteoprogenitor cells: An in-vitro study. *World J. Stem Cells*. **6** (4), 497–504. 10.4252/wjsc.v6.i4.497 (2014). From NLM PubMed-not-MEDLINE.
4. Perez-Herrero, E. et al. New injectable two-step forming hydrogel for delivery of bioactive substances in tissue regeneration. *Regen Biomater.* **6** (3), 149–162. 10.1093/rb/rbz018 (2019). From NLM PubMed-not-MEDLINE.
5. Faccendini, A. et al. Norfloxacin-Loaded Electrospun Scaffolds: Montmorillonite Nanocomposite vs. Free Drug. *Pharmaceutics* **12** (4). DOI: (2020). 10.3390/pharmaceutics12040325 From NLM PubMed-not-MEDLINE.
6. Freeman, F. E. et al. J. 3D bioprinting spatiotemporally defined patterns of growth factors to tightly control tissue regeneration. *Sci. Adv.* **6** (33), eabb5093. 10.1126/sciadv.abb5093 (2020). From NLM PubMed-not-MEDLINE.
7. Gonzalez-Sanchez, Z. et al. Titanium Surface Characteristics Induce the Specific Reprogramming of Toll-like Receptor Signaling in Macrophages. *Int. J. Mol. Sci.* **23** (8). 10.3390/ijms23084285 (2022). From NLM Medline.
8. Li, G. & Zhao, L. Sorafenib-loaded hydroxyethyl starch-TG100-115 micelles for the treatment of liver cancer based on synergistic treatment. *Drug Deliv*. **26** (1), 756–764. 10.1080/10717544.2019.1642418 (2019). From NLM Medline.
9. He, J. et al. Bioprinting of a Hepatic Tissue Model Using Human-Induced Pluripotent Stem Cell-derived Hepatocytes for Drug-Induced Hepatotoxicity Evaluation. *Int. J. Bioprint*. **8** (3), 581. 10.18063/ijb.v8i3.581 (2022). From NLM PubMed-not-MEDLINE.
10. de Melo, B. A. G. et al. 3D Printed Cartilage-Like Tissue Constructs with Spatially Controlled Mechanical Properties. *Adv. Funct. Mater.* **29** (51). 10.1002/adfm.201906330 (2019). From NLM PubMed-not-MEDLINE.
11. Lai, J. Y., Luo, L. J. & Ma, D. H. Effect of Cross-Linking Density on the Structures and Properties of Carbodiimide-Treated Gelatin Matrices as Limbal Stem Cell Niches. *Int. J. Mol. Sci.* **19** (11). 10.3390/ijms19113294 (2018). From NLM Medline.
12. He, J. et al. Obacunone targets macrophage migration inhibitory factor (MIF) to impede osteoclastogenesis and alleviate ovariectomy-induced bone loss. *J. Adv. Res.* **53**, 235–248. 10.1016/j.jare.2023.01.003 (2023). From NLM Medline.
13. Park, K. R., Kim, S., Cho, M. & Yun, H. M. Limonoid Triterpene, Obacunone Increases Runt-Related Transcription Factor 2 to Promote Osteoblast Differentiation and Function. *Int. J. Mol. Sci.* **22** (5). 10.3390/ijms22052483 (2021). From NLM Medline.
14. Weng, Y. et al. 3D-Printed Biomimetic Hydroxyapatite Composite Scaffold Loaded with Curculigoside for Rat Cranial Defect Repair. *ACS Omega*. **9** (24), 26097–26111. 10.1021/acsomega.4c01533 (2024). From NLM PubMed-not-MEDLINE.

15. Baek, S. K., Kim, S. & Song, K. B. Characterization of Ecklonia cava Alginate Films Containing Cinnamon Essential Oils. *Int. J. Mol. Sci.* **19** (11). 10.3390/ijms19113545 (2018). From NLM Medline.
16. Yao, Q., Liu, Y., Selvaratnam, B., Koodali, R. T. & Sun, H. Mesoporous silicate nanoparticles/3D nanofibrous scaffold-mediated dual-drug delivery for bone tissue engineering. *J. Control Release*. **279**, 69–78. 10.1016/j.jconrel.2018.04.011 (2018). From NLM Medline.
17. Zheng, C. et al. 3D-printed HA15-loaded beta-Tricalcium Phosphate/Poly (Lactic-co-glycolic acid) Bone Tissue Scaffold Promotes Bone Regeneration in Rabbit Radial Defects. *Int. J. Bioprint*. **7** (1), 317. 10.18063/ijb.v7i1 (2021). 317 From NLM PubMed-not-MEDLINE.
18. Wei, Y. et al. miR-424-5p shuttled by bone marrow stem cells-derived exosomes attenuates osteogenesis via regulating WIF1-mediated Wnt/beta-catenin axis. *Aging (Albany NY)*. **13** (13), 17190–17201. 10.18632/aging.203169 (2021). From NLM Medline.
19. Tan, Y. et al. Fabrication of a three-dimensional printed gelatin/sodium alginate/nano-attapulgite composite polymer scaffold loaded with leonurine hydrochloride and its effects on osteogenesis and vascularization. *Int. J. Biol. Macromol.* **249**, 126028. 10.1016/j.ijbiomac.2023.126028 (2023). From NLM Medline.
20. Fan, S. et al. Regulation of the immune microenvironment by pioglitazone-loaded polylactic glycolic acid nanosphere composite scaffolds to promote vascularization and bone regeneration. *J. Tissue Eng.* **15**, 20417314241231452 (2024). 10.1177/20417314241231452 From NLM PubMed-not-MEDLINE.
21. Unagolla, J. M. & Jayasuriya, A. C. Enhanced cell functions on graphene oxide incorporated 3D printed polycaprolactone scaffolds. *Mater. Sci. Eng. C Mater. Biol. Appl.* **102**, 1–11. 10.1016/j.msec.2019.04.026 (2019). From NLM Medline.
22. Kim, J., Jayaprakasha, G. K. & Patil, B. S. Obacunone exhibits anti-proliferative and anti-aromatase activity in vitro by inhibiting the p38 MAPK signaling pathway in MCF-7 human breast adenocarcinoma cells. *Biochimie* **105**, 36–44. 10.1016/j.biochi.2014.06.002 (2014). From NLM Medline.
23. Aragon-Navas, A. et al. Mimicking chronic glaucoma over 6 months with a single intracameral injection of dexamethasone/fibronectin-loaded PLGA microspheres. *Drug Deliv*. **29** (1), 2357–2374. 10.1080/10717544.2022.2096712 (2022). From NLM Medline.
24. Santschi, M. X. T. et al. Mechanical and Biological Evaluation of Melt-Electrowritten Polycaprolactone Scaffolds for Acetabular Labrum Restoration. *Cells* **11** (21). DOI: (2022). 10.3390/cells11213450 From NLM Medline.
25. Wang, Z. et al. C. 3D-printable self-healing and mechanically reinforced hydrogels with host-guest non-covalent interactions integrated into covalently linked networks. *Mater. Horiz*. **6** (4), 733–742 (2019). 10.1039/C8MH01208C From NLM PubMed-not-MEDLINE.
26. Li, X., Wang, C., Yang, S., Liu, P. & Zhang, B. Electrospun PCL/mupirocin and chitosan/lidocaine hydrochloride multifunctional double layer nanofibrous scaffolds for wound dressing applications.

Int. J. Nanomed. **13**, 5287–5299 (2018). 2147/IJN.S177256 From NLM Medline.

27. Wang, L. et al. N-carboxymethyl chitosan/sodium alginate composite hydrogel loading plasmid DNA as a promising gene activated matrix for in-situ burn wound treatment. *Bioact Mater.* **15**, 330–342. 10.1016/j.bioactmat.2021.12.012 (2022). From NLM.
28. Gao, M. et al. Construction of Double-Shelled Hollow Ag(2)S@Polydopamine Nanocomposites for Fluorescence-Guided, Dual Stimuli-Responsive Drug Delivery and Photothermal Therapy. *Nanomaterials (Basel)* **12** (12). DOI: (2022). 10.3390/nano12122068 From NLM PubMed-not-MEDLINE.
29. Li, Q., Zhou, H., Wang, C. & Zhu, Z. Long non-coding RNA Linc01133 promotes osteogenic differentiation of human periodontal ligament stem cells via microRNA-30c / bone gamma-carboxyglutamate protein axis. *Bioengineered* **13** (4), 9602–9612. 10.1080/21655979.2022.2054912 (2022). From NLM Medline.
30. Chi, H. et al. 3D-HA Scaffold Functionalized by Extracellular Matrix of Stem Cells Promotes Bone Repair. *Int. J. Nanomed.* **15**, 5825–5838 (2020). 10.2147/IJN.S259678 From NLM Medline.

Scheme

Scheme 1 is available in the Supplementary Files section.

Figures

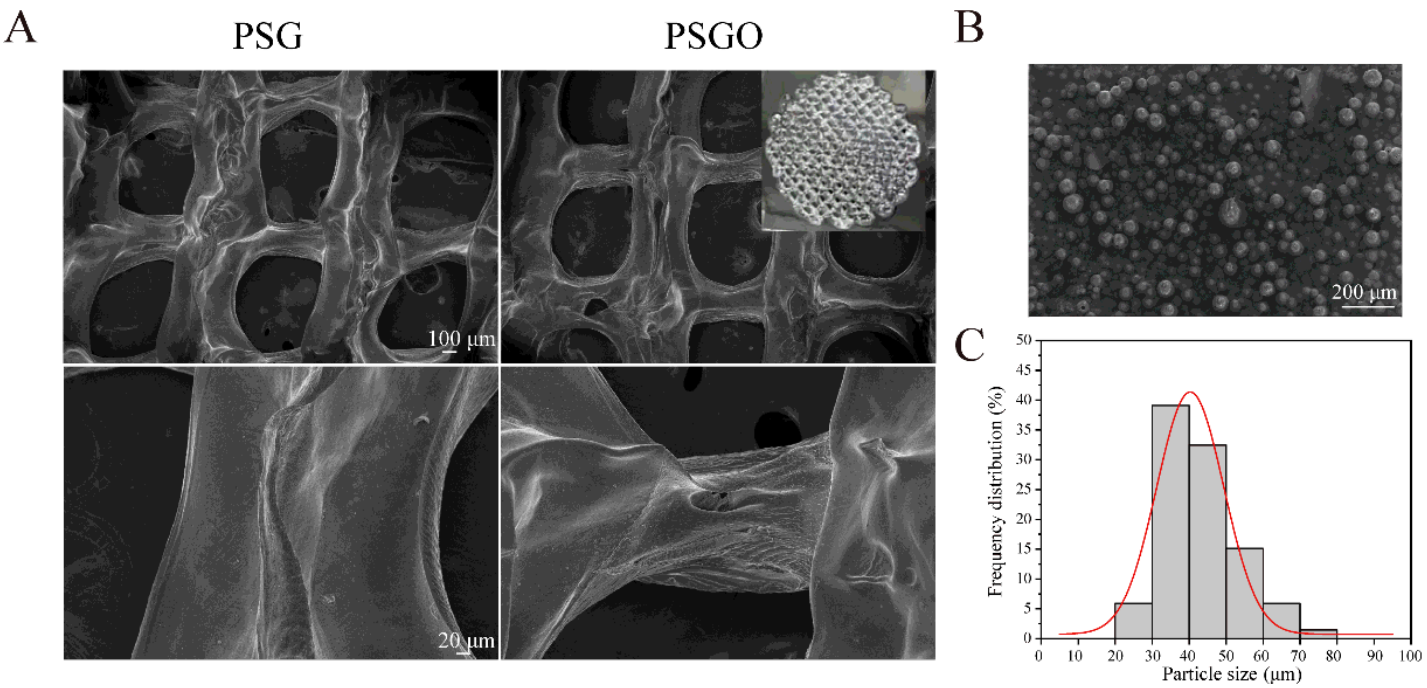

Figure 1

Microscopic Characterization of Materials. (A) Scanning electron microscopy (SEM) images and physical image of the scaffold. (B) SEM image of OA@PM microspheres. (C) Particle size distribution of OA@PM microspheres.

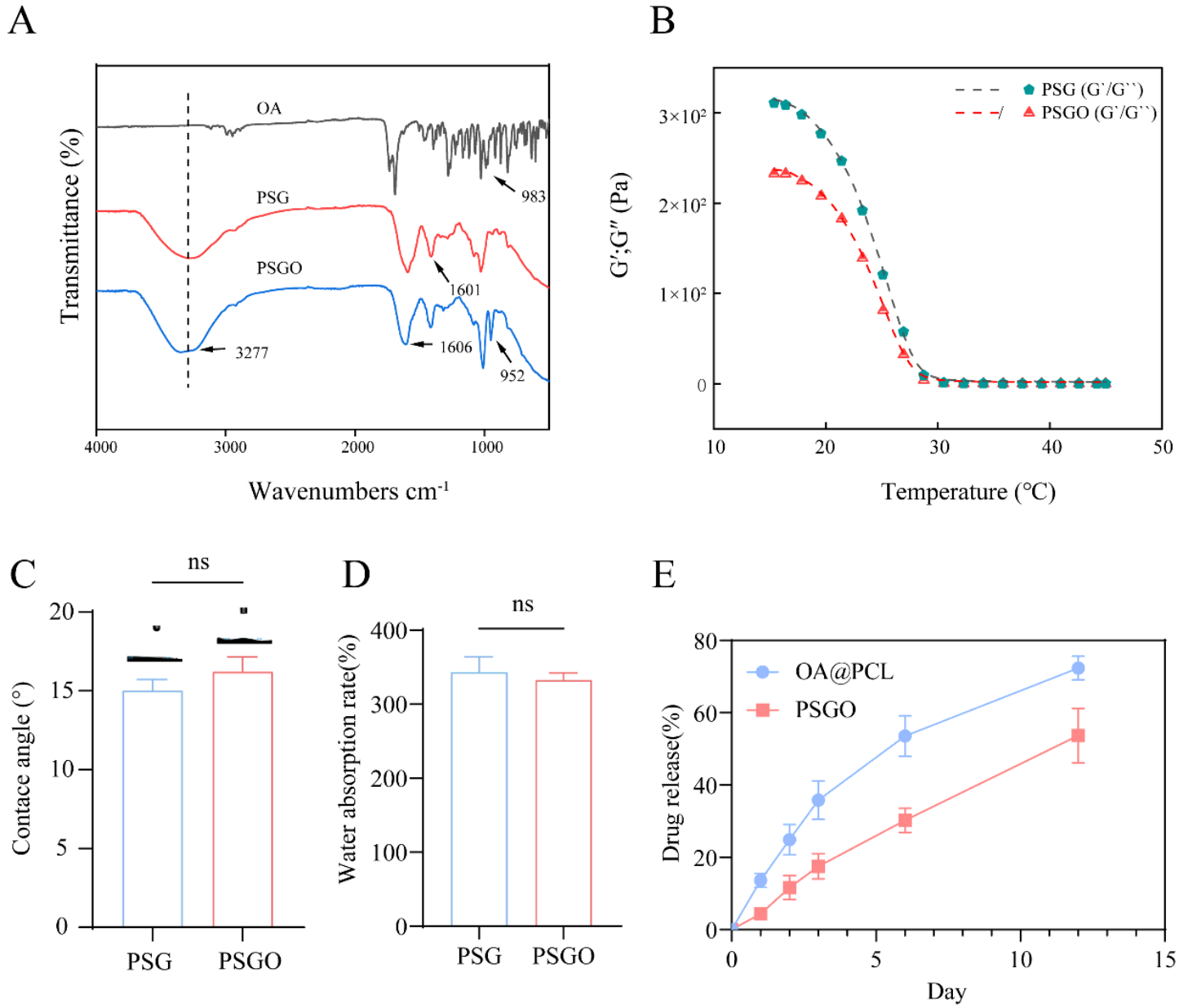

Figure 2

Composition and Physicochemical Properties of the Scaffolds. (A) FTIR spectra of different scaffolds. (B) Rheological analysis of the scaffolds. (C) Contact angle measurements and results of the scaffold hydrogel surface. (D) Water absorption rate of the scaffolds. (E) Evaluation of Obacunone release rate from OA@PM and PSGO scaffolds.

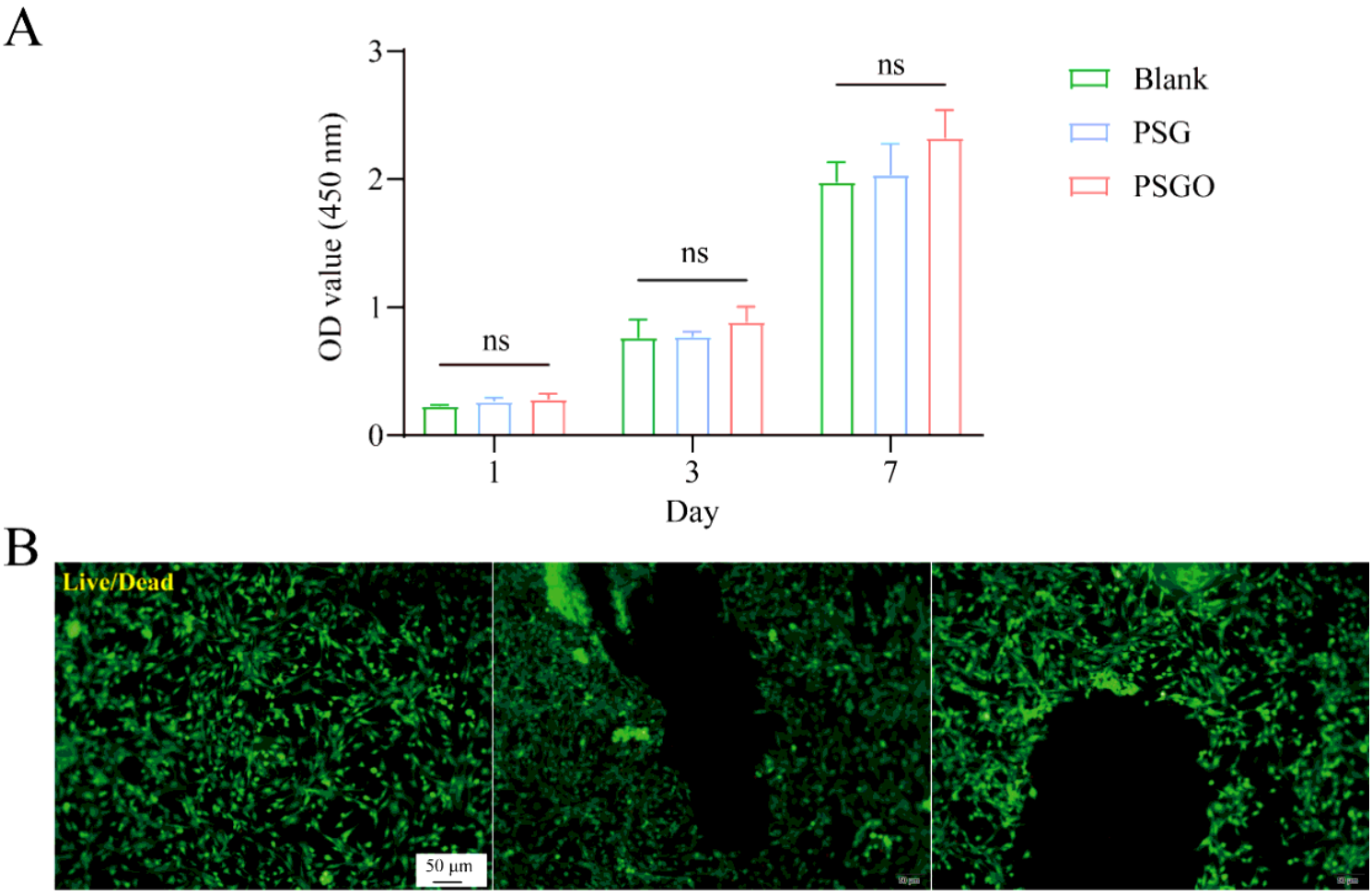

Figure 3

Biotoxicity and Biocompatibility of Hydrogel Scaffolds. (A) Quantitative analysis of cell viability after culturing PSG/PSGO composite hydrogels for 1, 3, and 7 days (n = 3). (B) Live/Dead fluorescence staining images after culturing the two scaffold groups for 2 days (n = 3).

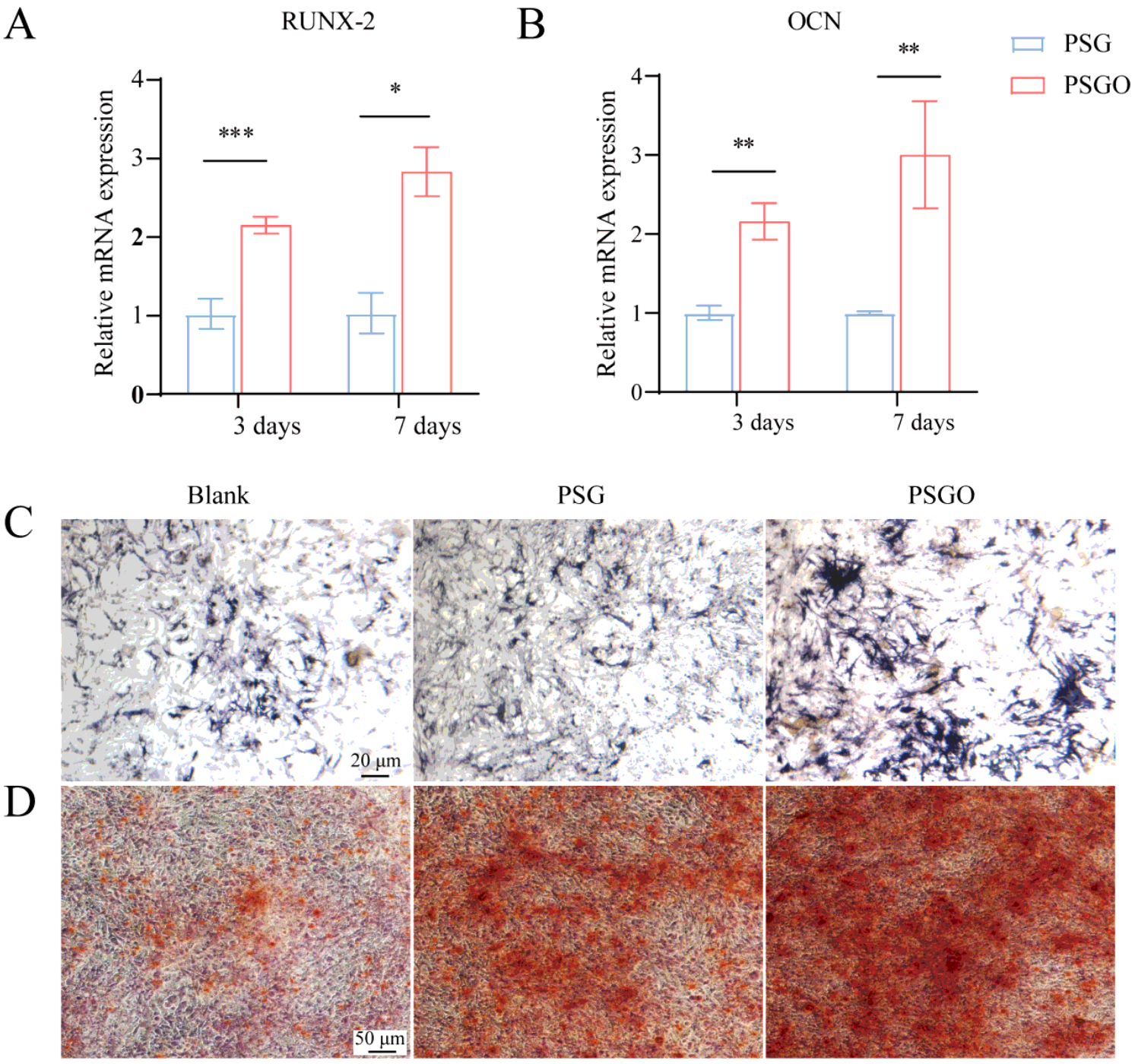

Figure 4

In vitro Evaluation of Osteogenic Activity of the Materials.

(A, B) Osteogenesis-related gene expression on days 3 and 7: (A) RUNX-2, (B) OCN ($^{*}P < 0.05$, $^{**}P < 0.01$, $^{***}P < 0.001$, n = 3); (C, D) ALP and ARS staining images of BMSCs co-cultured with material eluates.

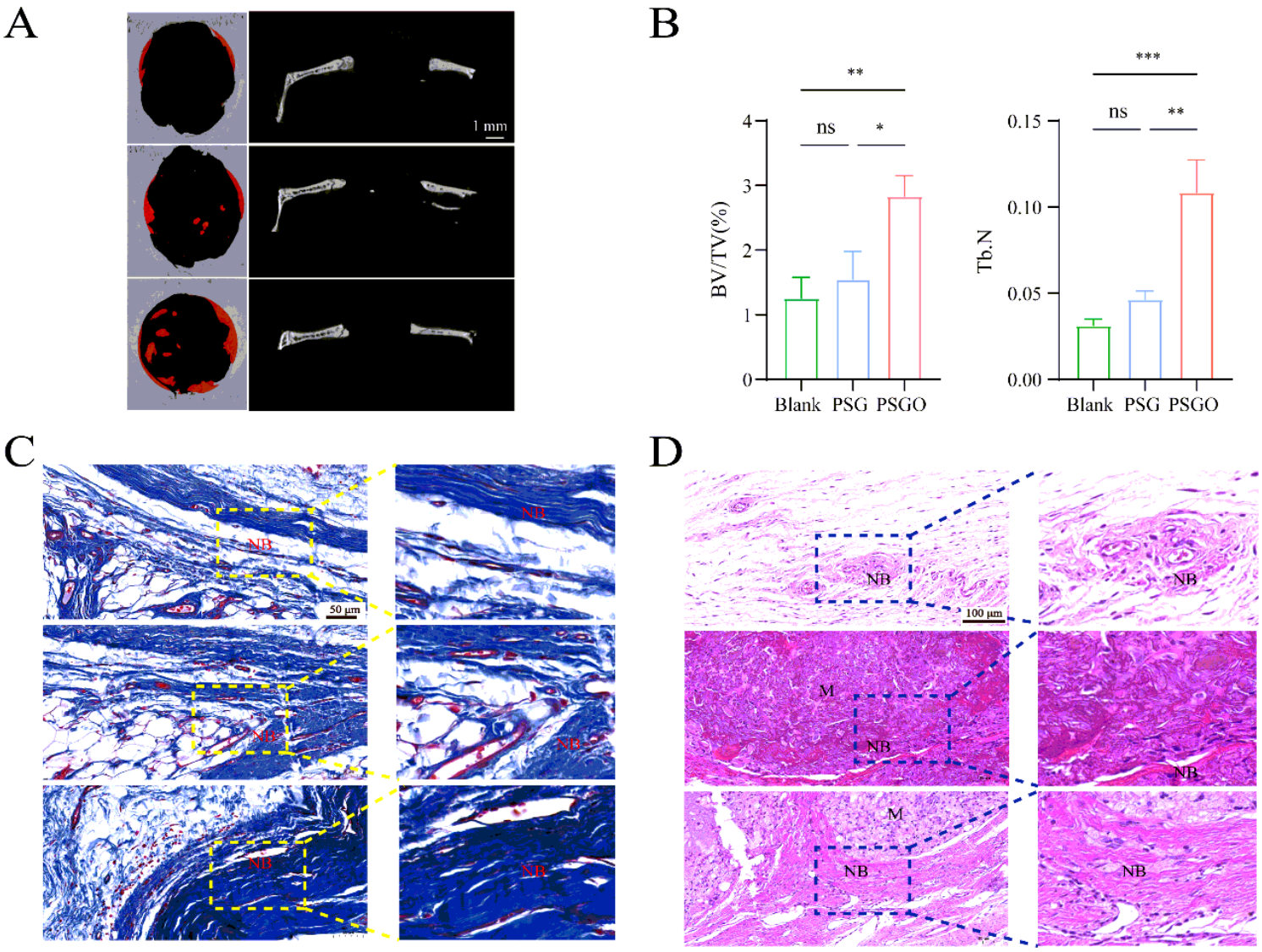

Figure 5

Imaging and Histological Evaluation at 4 Weeks Post-Surgery. (A) Micro-CT scanning and sagittal reconstruction images; (B) Quantitative analysis of bone volume fraction and trabecular number; (C and D) H&E staining images; Masson's trichrome staining images (NB = new bone, M = composite scaffold).

Supplementary Files

This is a list of supplementary files associated with this preprint. Click to download.

- floatimage1.png